RSC Advances

g-C3N4 hybridized with AgVO3 nanowires: Preparation and its Enhanced visible-light-induced photocatalytic activity

Journal:	*RSC Advances*
Manuscript ID:	RA-ART-05-2015-008367.R1
Article Type:	Paper
Date Submitted by the Author:	19-May-2015
Complete List of Authors:	Shi, Haifeng; Jiangnan University, Zhang, Chengliang; jiangnan University,, Zou, Changping; Jiangnan university,

g-C_3N_4 hybridized with $AgVO_3$ nanowires: Preparation and its Enhanced visible-light-induced photocatalytic activity

Haifeng Shi, [a,b *] Chengliang Zhang ,[a,b] and Changping Zhou [a,b]

[a] School of science, Jiangnan University, Wuxi, P. R. China, 214122.

[b] Jiangsu Provincial Research Center of Light Industrial Optoelectronic Engineering and Technology, Jiangnan University, Wuxi, P. R. China, 214122.

Abstract: The g-C_3N_4/$AgVO_3$ nanowires composite were fabricated and developed to an efficient visible-light-induced photocatalyst for eliminating the organic pollutants. The phase compositions, optical properties, and morphologies of the composite photocatalysts were systematically characterized via powder X-ray diffraction, scanning electron microscopy, high-resolution transmission electron microscopy, UV-vis diffuse reflection spectroscopy, BET measurement, X-ray photoelectron spectroscopy, and photoluminescence spectroscopy. Compared with single-phase g-C_3N_4 and $AgVO_3$ nanowires, the g-C_3N_4/$AgVO_3$ nanowires composite photocatalysts displayed much higher photocatalytic activity for rhodamine B degradation under visible-light irradiation. The optimal mass ratio of g-C_3N_4 to $AgVO_3$ content for rhodamine B photodegradation activity of the composite structures was determined. Particularly, the photocatalytic activity of the g-C_3N_4/0.2$AgVO_3$

*Corresponding author. E-mail address: shihaifengnju@hotmail.com (HF Shi)

nanowires composite for the degradation of RhB was almost 3.0 and 3.5 times higher than those of g-C_3N_4 and $AgVO_3$ nanowires, respectively. The notably increased photocatalytic activity of g-$C_3N_4/AgVO_3$ could be attributed to the enhanced the photoinduced electron−hole separation efficiency in $Ag/C_3N_4/AgVO_3$.

Keywords: Graphitic carbon nitride, silver vanadate, composite photocatalyst, nanowires, charge transfer.

1. Introduction

The rapidly increasing production of toxic pollutants or organic contaminants with industrial development and population expansion is becoming one of the most stubborn issues in view of the serious environmental problems facing mankind. Photocatalysis technique using semiconductors and solar light, as a cost-effective and environmental technology, has been widely applied to the treatment of wastewater or gaseous contaminants due to the reduction and oxidation ability of the photoinduced electrons and holes in semiconductors [1–11]. Especially, the photodegradation of organic dyes has become one of the hot topics for environment remediation since biodegradation is not efficient enough to eliminate dyestuffs [12–16]. During the past four decades, TiO_2 has been extensively investigated as a classic photocatalyst due to the advantages of chemical stability and nontoxic. However, the relative wide band gap wide limits it only active under the ultraviolet (UV) light irradiation. Thus the development of visible-light sensitive photocatalysts is obviously necessary for future applications in the view of effective utilization of sunlight or indoor artificial illuminations.

Up to now, two avenues are generally applied to develop visible-light driven

photocatalysts. One method is the modification of TiO_2 by the following strategies, such as metal-ion or non-metal doping, semiconductors coupling and dye sensitization [17–19]. Another method is the development of new and efficient visible-light sensitive semiconductors [20-24]. Recently, it has been shown that silver vandate ($AgVO_3$) possesses excellent photocatalytic properties owing to the highly dispersed hydride valence band (Ag 4d + O 2p) and narrow band gap since Konta et al reported that $AgVO_3$ showed a photocatalytic activity for O_2 evolution from an aqueous silver nitrate solution[25]. Moreover, the photocatalytic activity of $AgVO_3$ could be further improved through the strategies, such as morphology modulation and noble metal loading [26-29]. However, the activity of pure $AgVO_3$ is still low and needs to be modified to improve the photocatalytic performance under visible light irradiation. Among the various methods to improve the photocatalytic performance, constructing heterostructured composites by combining two different catalysts with suitable conduction and valence bands is generally considered as one of the promising methods owing to increasing the photogenerated charge separation efficiency and enhancing the visible light absorption.

Recently, a typical metal-free π-conjugated semiconductor, graphitic carbon nitride (g-C_3N_4) with high thermal and chemical stability, has obtained a great deal of scientific interest owing to its potential in photocatalytic splitting of water, organic pollutant degradation, and CO_2 reduction [30-34] ever since the first discovery of its photocatalytic activity for hydrogen production [35]. Unfortunately, the photocatalytic efficiency of the pure g-C_3N_4 is limited due to the high recombination rate of the photo-generated electron–hole pairs, which is usually considered as a major barrier in the single-component semiconductor photocatalyst. In view of the benefits of constructing composite composites, several g-C_3N_4-based composite photocatalysts

have been successfully developed and displayed significantly higher photocatalytic activity than that of the pristine material comprising the composites, which has been demonstrated in the photodegradation of organic pollutants, CO_2 reduction and water splitting [36-43].

It is generally acknowledged that the one-dimensional nono-materials generally provide larger surface-to-volume ratios available and possess more efficient ballistic charge transport along the single nanowires than the diffusive transport in powdered materials [44-46]. Now the question is whether g-C_3N_4 and $AgVO_3$ nanowires are two appropriate candidates for constructing a nano-heterostructured photocatalyst to work under visible-light irradiation? The present work has given a clear and positive answer. In this study, we synthesized a novel heterostructured photocatalyst based on $AgVO_3$ nanowires and g-C_3N_4 via a solid calcination method. The physical characteristics of samples were examined by the techniques, such as XRD, UV-vis diffuse reflectance spectroscopy, FE-SEM, TEM, BET measurement, XPS, and photoluminescence (PL) spectra. Rhodamine B (RhB) was used as a model organic pollutant to evaluate the photocatalytic activities of samples under visible light irradiation. In contrast to g-C_3N_4 and $AgVO_3$ nanowires, g-C_3N_4/$AgVO_3$ nanowires composite exhibited a much higher activity of photocatalytic RhB degradation under visible-light irradiation. The effects of different mass ratio on photocatalytic activity were systematically investigated. The possible mechanism of the enhanced activity of the photocatalyst was proposed in view of the efficient separation and transport of charge carriers.

2. Experimental

2.1 Synthesis of photocatalysts

All chemical reagents were of analytical pure grade and used as received without

further purification. Silver vanadate (β-$AgVO_3$) nanowires were synthesized through a hydrothermal treatment method. In a typical case, 2.5 mmol ammonium metavanadate precursor (NH_4VO_3, Aldrich) precursor and 0.50 g of P123 (BASF, USA) were dissolved in distilled water (30 mL) containing 1 M HNO_3 (2 mL). Subsequently, this mixture was placed at room temperature for 7 h with magnetic stirring, followed by addition of 2.5 mmoL of silver nitrate ($AgNO_3$, Wako). After being constantly stirred for 1 h, the mixture was poured into a 50 mL Teflon-lined autoclave and then maintained at 170 ◦C for 24 h. After cooling to room temperature, the obtained precipitate was washed thoroughly with a distilled water and acetone several times and dried in an oven at 70 ℃ for 12 h. The metal-free g-C_3N_4 powders were synthesized by heating melamine in a muffle furnace. In a typical process, 10 g of melamine was placed in a crucible with a cover. The crucible was heated to 520 ℃ for 4 h at a heating rate of 20 ℃ min^{-1}. The product g-C_3N_4 was naturally cooled to room temperature and ground into powders. The g-C_3N_4/$AgVO_3$ nanowires composites were prepared as follows: firstly, the methanol solution containing g-C_3N_4 powder was ultrasonicated for 30 min in order to completely disperse g-C_3N_4. Subsequently, the as-prepared $AgVO_3$ nanowires powder was added into the above suspension and constantly stirred for 24 h. After that, the product was washed with distilled water and dried in an oven at 70 ℃ for 24 h. Finally, the obtained samples were heated to 250 ℃ for 1 h. The different mass ratios of g-C_3N_4/$AgVO_3$ composite photocatalysts were synthesized according to the similar method as mentioned above. The weight ratios of g-C_3N_4 to $AgVO_3$ were 0.9:0.1, 0.8:0.2, and 0.7:0.3, which were denoted as g-C_3N_4/0.1$AgVO_3$, g-C_3N_4/0.2$AgVO_3$, and g-C_3N_4/0.3$AgVO_3$, respectively.

2.2 Characterization

Powder X-ray diffraction studies were characterized by an X-ray diffractometer (DX2700, Haoyuan Instrument Co., Ltd., Dandong, China) using Cu Kα radiation in the 2θ ranging from 10˚ to 80˚. The diffuse reflectance spectra of the sample were conducted in the range of 300-850 nm using a UV-vis spectrophotometer (UV-2600; Shimadzu, Japan), equipped with an integrating sphere attachment and a reference ($BaSO_4$). Morphologies of samples were measured by a field-emission scanning electron microscope (FE-SEM; FEI Tecnai G2 F30, USA) and a high resolution transmission electron microscope (HRTEM, JEM-2010, JEOL, Japan). The specific surface areas were deduced according to Brunauer-Emmett-Teller method using a surface area and porosimetry analyzer (V-sorb 2800, Gold APP, China) at 77 K. Photoluminescence (PL) spectra were measured at room temperature on a fluorescence spectrophotometer (FLS920P, Edinburgh, England) with an excitation wavelength of 350 nm. X-ray photoelectron spectroscopy (XPS) analysis was conducted on a multifunctional imaging electron spectrometer (Thermo ESCALAB 250XI, USA) using an Al Kα monochromatic X-ray radiation.

2.3 Photocatalytic reaction

The photocatalytic activities of the g-$C_3N_4/AgVO_3$ composite samples were evaluated by photodegradation of rhodamine B (RhB) dye in an aqueous solution under visible-light irradiation. The catalyst (0.1 g) was firstly dispersed in RhB aqueous solution (100 mL, 4 mg L^{-1}). Prior to irradiation, the photocatalysts was suspended in the solution with magnetically stirring for 60 min under dark condition to ensure that the surface of photocatalysts was saturated with RhB. The light was

irradiated from a 300 W Xe-lamp with cut-off filter L42. The variation in RhB concentration was examined by absorbance intensity through a UV–vis spectrophotometer (UV 2600, Shimadzu, Japan). As references, the photocatalytic activity of the pure g-C_3N_4 and pure $AgVO_3$ nanowires were evaluated under the same conditions.

3. Results and Discussion

3.1. Characterization of g-C_3N_4/$AgVO_3$ nanowires composites.

The phase of the as-prepared g-C_3N_4, $AgVO_3$, and g-C_3N_4/$AgVO_3$ composite photocatalysts were checked by XRD, and the typical diffraction patterns are shown in Fig. 1. The diffraction peaks of $AgVO_3$ sample could be indexed to a monoclinic-structured $AgVO_3$, in good agreement with those in the JCPDS Card (No. 00-029-1154), and no other obvious peaks from possible impurities were detected. The strong peak at 27.4º of the g-C_3N_4 sample could be indexed as (100) diffraction planes of g-C_3N_4 (JCPDS 87-1526), corresponding to the characteristic interplanar staking peaks of aromatic systems. As for g-C_3N_4/$AgVO_3$ composites, the XRD patterns revealed the coexistence peaks of $AgVO_3$ and g-C_3N_4 phases. It was noted that the characteristic peaks of $AgVO_3$ (28.4º) and g-C_3N_4 (27.4º) were too close to obviously distinguish. Nevertheless, the diffraction peaks (28.4º) corresponding to $AgVO_3$ appeared and increased the peak intensity with the increasing content of $AgVO_3$ from 10 wt% to 30 wt%. The XRD results implied co-existence of g-C_3N_4 and $AgVO_3$ in the g-C_3N_4/$AgVO_3$ composite materials.

Fig. 2a displays the UV–vis diffuse reflectance spectra of g-C_3N_4, $AgVO_3$, and g-C_3N_4/$AgVO_3$ composite photocatalysts. The absorption threshold of g-C_3N_4 was

approximately at 450 nm, whereas the absorption edge of $AgVO_3$ was estimated to be 550 nm. It was noted that the absorption spectra of g-C_3N_4/$AgVO_3$ samples exhibited a slight red shift of the g-C_3N_4 and a shoulder on the adsorption edge that reached further out in the visible region, which were attributed to the interaction between g-C_3N_4 and $AgVO_3$ in the composite samples. In addition, the spectral range increased with the increase of the $AgVO_3$ nanowires content. As a result, this clearly demonstrated that the spectral response of the g-C_3N_4/$AgVO_3$ had potential applications under visible-light irradiation. The optical band gap E_g of a semiconductor could be deduced according to the following equation $(\alpha hv)^n = A\ (hv - E_g)$, where α means the absorption coefficient, hv is the incident photo energy, the value of the index n depends on the electronic transition of the semiconductor (n_{direct} = 2; $n_{indirect}$ = 1/2), A is a proportionality constant related to the material, and E_g is the band gap energy of the semiconductor, respectively. As shown in Fig. 2b, the band gap energies of g-C_3N_4 and $AgVO_3$ were obtained from the intercept of the tangent line in the plot of $(\alpha hv)^{1/2}$ versus energy to be 2.7 eV and 2.2 eV, respectively.

Fig. 3 shows the X-ray photoelectron spectroscopy (XPS) spectra of C 1s and N 1s spectra of g-C_3N_4 and g-C_3N_4/0.2$AgVO_3$, as well as V 2p, Ag 3d and O 1s for $AgVO_3$ and g-C_3N_4/0.2$AgVO_3$ heterojunctions. The XPS spectra were calibrated using the C-C bonds at 284.6 eV. As displayed in the high resolution XPS spectra of C 1s (Fig. 3a), the two peaks (284.6 eV and 288.0 eV) in g-C_3N_4 corresponded to sp^2 C–C bonds and sp^2-bonded carbon in N-containing aromatic rings (N–C=N), respectively [47,48]. While g-C_3N_4/0.2$AgVO_3$ composite showed higher binding energies of C 1s (284.6 eV and 288.3 eV) compare with pure g-C_3N_4. The inner shift of C 1s peak possibly originated form hybridized effect between g-C_3N_4 and $AgVO_3$

nanowires. The binding energy of N 1s of g-C_3N_4/0.2$AgVO_3$ was located at 398.8 eV, while the corresponding peak of g-C_3N_4 was 398.9 eV [49]. As shown in Fig. 3c.d, the binding energies of Ag $3d_{5/2}$ (373.8 eV), Ag $3d_{3/2}$ (367.8 eV) and O 1s (529.8 eV) for $AgVO_3$ were similar to those of Ag $3d_{5/2}$ (373.6 eV), Ag $3d_{3/2}$ (367.6 eV) and O 1s (529.7 eV) for g-C_3N_4/0.2$AgVO_3$. Additionally, the binding energies of V $2p_{3/2}$ (516.6 eV) and V $2p_{1/2}$ (524 eV) for $AgVO_3$ were lower than those of V $2p_{3/2}$ (517 eV) and V $2p_{1/2}$ (524.5 eV) for g-C_3N_4/0.2$AgVO_3$. Hence it implied that g-C_3N_4 and $AgVO_3$ possibly had interaction in structure to form the composite [50]. Furthermore, the BET surface area of g-C_3N_4, g-C_3N_4/0.2$AgVO_3$, and β-$AgVO_3$ nanowires were measured to be 6.5, 7.9, and 12.8 m^2/g using the nitrogen adsorption-desorption measurement, respectively.

The morphologies and microstructures of g-C_3N_4, $AgVO_3$, and g-C_3N_4/0.2$AgVO_3$ composite samples were investigated by FE-SEM. As indicated in Fig. 4a, the large amount of aggregated lamellar structures with several stacking layers can be observed for g-C_3N_4. The $AgVO_3$ sample displays a number of nanowires with a diameter of ~20 nm and length of up to several tens micrometers (Fig. 4b). As shown in Fig. 4c, after combining g-C_3N_4, $AgVO_3$ nanowires (with slight Ag nanoparticles) not only remains the similar morphology to the pristine $AgVO_3$ nanowires but also randomly distributes with g-C_3N_4 and thus constructs a composite material. Aiming at obtaining farther microstructures information of the g-C_3N_4/0.2$AgVO_3$, the transmission electron microscopy (TEM) analysis was applied. Fig. 5 depicts the low- and high-magnification transmission electron microscopy images of the as-prepared g-C_3N_4/0.2$AgVO_3$ composite. On the basis of the SEM image of $AgVO_3$ nanowires, the dark parts in the TEM image (Fig. 5a) should be

$AgVO_3$ nanowires while the light parts correspond to g-C_3N_4. The intimate interfaces are evidently displayed between the g-C_3N_4 and $AgVO_3$, which further implies the formation of g-C_3N_4 and $AgVO_3$ composites. From the HRTEM image of g-C_3N_4/0.2$AgVO_3$ composite (Fig. 5b), the clear lattice fringe should be ascribed to $AgVO_3$, and the d spacing value was 0.230 nm corresponding to the (312) plane of monoclinic-structured $AgVO_3$, while the low crystallinity with blurry lattices is ascribed to g-C_3N_4. [38] Moreover, this result suggests that g-C_3N_4/$AgVO_3$ is heterogeneous-composited structure rather than a simply physical mixture of two separate phases of g-C_3N_4 and $AgVO_3$. The observed intimate interface is generally expected to be favorable for the photoinduced carriers rapidly transfer between g-C_3N_4 and $AgVO_3$.

3.2. Photocatalytic activity of g-C_3N_4/$AgVO_3$ composite.

The photocatalytic activities of samples were evaluated for the photodegradation of RhB solution upon visible-light irradiation. The degradation rate of RhB was examined by characteristic absorption peak at 554 nm. Fig. 6 displays the C/C_0 *vs* irradiation time over g-C_3N_4, $AgVO_3$, physically mixed g-C_3N_4-$AgVO_3$, and g-C_3N_4/0.2$AgVO_3$ nanowires composite photocatalysts under visible-light illumination. It can be seen that, after 60 min of visible light illumination, RhB removal rate over $AgVO_3$ nanowires is ~ 65%, while g-C_3N_4 shows a relatively high photocatalytic performance with a photodegradation ratio of 73%. After combining g-C_3N_4 with $AgVO_3$ nanowires, the photocatalytic activity of g-C_3N_4/0.2$AgVO_3$ composite photocatalysts significantly improved for the degradation of RhB compared with the pure g-C_3N_4 and $AgVO_3$. As a reference, g-C_3N_4 and $AgVO_3$ nanowires with the same weight ratio as g-C_3N_4/0.2$AgVO_3$ was physically mixed. It

can be seen from Fig. 6 that g-C_3N_4/0.2$AgVO_3$ composited photocatalysts showed a higher photocatalytic activity than physically mixed g-C_3N_4-$AgVO_3$, suggesting that the interaction between g-C_3N_4 and $AgVO_3$ plays a significant role in improving the photocatalytic activity. In addition, when the suspension was irradiated by visible-light without any photocatalyst (blank), there was no apparent change in the concentration of RhB, suggesting that RhB was difficult to be photolysis. The stability of the as-synthesized photocatalyst was performed over g-C_3N_4/0.2$AgVO_3$ composite for following recycling experiment. As shown in Fig. 7, RhB is quickly decolorized after each photodegradation experiment and only a slight decreasing loss of the photocatalytic activity of g-C_3N_4/0.2$AgVO_3$ is observed after three cycles. Furthermore, XRD patterns of g-C_3N_4/0.2$AgVO_3$ composite before and after the RhB degradation reaction are shown in Fig. 8. There was a new small peak appeared at ~ 38 degree in the XRD patterns, corresponding to Ag (111) peak. This indicated that Ag was formed after the photodegradation reaction. Actually, the transformation of Ag^+ into Ag^0 usually takes place in some silver containing semiconductors during the photocatalytic reaction process [51,52].

In order to quantitatively investigate the reaction kinetics of the RhB degradation (millimolar concentration), the experimental data was generally fitted by a pseudo-first-order model [53,54]

$$\ln(C_0/C) = kt \quad (1)$$

where k is the apparent reaction rate constant, C_0 means the adsorption equilibrium concentration of RhB, t represents the reaction time, and C is the concentration of RhB at the reaction time t. As shown in Fig. 9, all of the g-C_3N_4/$AgVO_3$ nanowires composite photocatalysts displayed higher photocatalytic degradation rates than pure

g-C_3N_4 and $AgVO_3$ nanowires. It could also be seen from Fig. 9 that the content of $AgVO_3$ influenced the photocatalytic activity of the as-prepared materials notably. Among the hybrid composites, g-C_3N_4/0.2$AgVO_3$ exhibited the highest photocatalytic activity for the decolorization of RhB. According to the first-order linear fitting, the apparent rate constant k was obtained and displayed in the inset of Fig. 9. The apparent rate constant k of g-C_3N_4/0.2$AgVO_3$ determined to be ~ 0.059 min^{-1}, which was 3.5 times and 3.0 times as high as that of the pure g-C_3N_4 and $AgVO_3$. At the same time, the k of g-C_3N_4/0.2$AgVO_3$ was 2.1-folds higher than that of physically mixed C_3N_4-$AgVO_3$. Additionally, g-C_3N_4/0.2$AgVO_3$ displayed the highest apparent rate constant k in the composite photocatalysts. This implied that the suitable weight ratio between $AgVO_3$ and g-C_3N_4 would create well dispersion in the composite, which facilitates to the transfer and separation of charge carriers and thus enhance the photocatalytic activity.

3.3. Possible photocatalytic mechanism of g-C_3N_4/$AgVO_3$ composite.

It is generally acknowledged that the photocatalytic activity of a semiconductor is intrinsically governed by the surface area, light absorption and electronic property. In the present case, the photocatalytic activities in the photodegradation of RhB are apparently different although g-C_3N_4/$AgVO_3$ and g-C_3N_4 have similar optical absorption and comparable surface areas. This suggests that there should be other crucial factors that greatly influence the photocatalytic activities. Actually, in addition to the optical absorption and surface area, the efficient charge separation of a semiconductor usually plays a crucial role in determining the photocatalytic

performance. In other words, the synergistic effect between the $AgVO_3$ and g-C_3N_4 is important to affect the photocatalytic property. Herein, band potentials of g-C_3N_4 and $AgVO_3$ were investigated in order to clarify the charge transport in the interfaces using the equation related to Mulliken electronegativity and the band gap of a semiconductor, which is describe by $E_{VB} = X - E_e + 0.5E_g$ [55-57], where E_{VB} and E_g are the top of valance band (VB) relative to the normal hydrogen electrode (NHE) and the band gap energy of the photocatalyst, respectively; E_e is the energy of free electrons (4.5 eV); X is the geometric mean of the Mulliken electronegativity of the constituent atoms in photocatalyst; and the conduction band (CB) can be obtained by $E_{CB} = E_{VB} - E_g$. Subsequently E_{VB} and E_{CB} of $AgVO_3$ are determined to be 2.46 eV and 0.26 eV relative to the normal hydrogen electrode (NHE), which was similar to the previous reports [58]. While the CB and VB edge potentials of g-C_3N_4 are calculated to be -1.13 eV and 1.57 eV, respectively. In addition, the valence band X-ray photoelectron spectroscopy (VB-XPS) was further preformed to investigate the VB top of g-C_3N_4 and $AgVO_3$. As shown in Figure 10, it could be seen that the positions of the valence band edge of g-C_3N_4 and $AgVO_3$ were located at ~ 1.6 and 2.3 eV, respectively, which were consistent with the theoretical calculated results. Herein, the photocatalytic mechanism for g-$C_3N_4/AgVO_3$ is tentatively proposed and illustrated in Fig. 11. Since the CB edge potential of g-C_3N_4 (-1.13 eV) is more negative than that of $AgVO_3$ (0.26 eV), the photoexcited electrons on g-C_3N_4 could transfer to the CB of $AgVO_3$ nanowires and Ag via the well developed interface due to the excellent conductivity and the electron storing capacity of the Ag nanoparticles [51]. Similarly,

the photoinduced holes on the $AgVO_3$ nanowires surface move towards g-C_3N_4 due to the difference in valence band edge potentials. In addition, the photogenerated electron−hole pairs are formed on the surface of Ag nanoparticles under visible-light irradiation owing to the localized surface plasmon resonance (SPR) effect from the collective oscillation of the surface electrons [59-63]. The photoinduced-electrons in Ag nanoparticles can participate in further reduction reactions. While the photoinduced-holes can move to the valence band of $AgVO_3$ and subsequently transfer to VB of g-C_3N_4, followed by oxidize the organic dyes [64,65]. In such an efficient way, the photoexcited electron–hole pairs could be effectively separated and thus enhance the photocatalytic activity. In addition, the morphologies and microstructures of photocatalysts could affect the performance notably. In the present case, the network structure of g-C_3N_4 generally provides an excellent electron transfer platform to facilitate the charge transport [66,67]. The $AgVO_3$ nanowires with larger surface-to-volume ratios available generally possess more efficient ballistic charge transport along the single nanowires than the diffusive transport in the corresponding powdered materials [68]. The above results reveal that the formation of composite combining C_3N_4 with $AgVO_3$ nanowires could enhance the photocatalytic activities under visible-light irradiation.

Photoluminescence (PL) spectra are applied to investigate the process of charge carrier trapping, migration, transfer and separation transfer. Fig. 12 displays the photoluminescence spectra of g-C_3N_4 and g-C_3N_4/0.2$AgVO_3$ composite photocatalysts with an excitation wavelength of 350 nm. It was observed that the main

emission peak of pure g-C_3N_4 was centered at ~ 460 nm, which was attributed to the band–band PL process of self-trapped excitations. It is generally acknowledged that the increasing recombination rate of electron hole pairs would lead to the higher fluorescence intensity. [1] As for the present case, the emission intensity of the g-C_3N_4/0.2$AgVO_3$ significantly decreased at the similar emission peak in g-C_3N_4, which indicates that the recombination rate of photogenerated charge carriers is lower in the g-C_3N_4/0.2$AgVO_3$ composite. The PL results clearly implied that the formation of interface between g-C_3N_4 and $AgVO_3$ possibly inhibited the recombination of photogenerated charge carriers.

4. Conclusions

A novel composite photocatalyst based on g-C_3N_4 and $AgVO_3$ was developed to efficient degradation of RhB under visible light irradiation. The transmission electron microscope and X-ray photo-electron spectroscopy results demonstrated that $AgVO_3$ nanowires well distributed with g-C_3N_4 and the g-C_3N_4/$AgVO_3$ composites were formed. The g-C_3N_4/$AgVO_3$ composite samples had a visible light absorption up to 540 nm. Compared with pure g-C_3N_4 and $AgVO_3$ nanowires, the g-C_3N_4/$AgVO_3$ nanowires hybrid materials displayed much higher photocatalytic activity for RhB degradation under visible-light irradiation. An optimal RhB photodegradation activity was found to be g-C_3N_4/0.2$AgVO_3$, which was nearly 3.0 and 3.5 times higher than those of either individual C_3N_4 or $AgVO_3$, respectively. This enhancement could be attributed to the high separation and easy transfer of photogenerated electron−hole

pairs at the intimate interface of composites, which can be reasonably ascribed to the enhanced the photoinduced electron−hole separation efficiency in $Ag/C_3N_4/AgVO_3$. In summary, the present research provides the promising application of inorganic–organic composite photocatalyst in the fields of organic pollutant degradation.

Acknowledgements

The authors would like to acknowledge the financial support from National Natural Science Foundation of China (Nos, 21203077, 51471077).

References

[1] M. R. Hoffmann, S. T. Martin, W. Choi, D. W. Bahnemann, *Chem. Rev.*, 1995, 95, 69-96.

[2] R. Asahi, T. Morikawa, T. Ohwaki, K. Aoki, Y. Taga, *Science*, 2001, 293, 269-271.

[3] J. Tang, Z. Zou, J. Ye, *Angew. Chem. Int. Ed.*, 2004, 43, 4463-4466.

[4] X. Chen, S. S. Mao, *Chem. Rev.*, 2007, 107, 2891-2959.

[5] G.Q. Li, N. Yang, W. L. Wang, W. F. Zhang, *J. Phys. Chem. C*, 2009, 113, 14829-14833.

[6] H. Xu, Y. Song, Y. Song, J. Zhu, T. Zhu, C. Liu, D. Zhao, Q. Zhang, H. M.Li , *RSC Adv*., 2014, 4, 34539–34547

[7] K. Fuku, R. Hayashi, S. Takakura, T. Kamegawa, K. Mori, H. Yamashita, *Angew. Chem. Int. Ed.*, 2013, 52, 7446-7450.

[8] W. J. Liu, X. Liu, Y.H. Fu, Q. You, R. Huang, P. Liu, Z.H. Li, *Appl. Catal. B: Environ,* 2014, 123, 78-83.

[9] J. S. Jang, H. G. Kim, J. S. Lee, *Catal. Today,* 2012, 185, 270-277.

[10] M. Zhang, C. Chen, W. Ma, J. C. Zhao, *Angew. Chem. Int. Ed.*, 2008, 47, 4516-4520.

[11] R. A. Lucky, P. A. Charpentier, *Adv. Mater.*, 2008, 20, 1755-1759.

[12] H. B. Fu, C. S. Pan, W. Q. Yao, Y. F. Zhu, *J. Phys. Chem. B*, 2005, 109, 22432-22439.

[13] X. K. Li, N. Kikugawa, J. H. Ye, *Chem. Eur. J.*, 2009, 15, 3538-3545.

[14] W. F. Yao, B. Zhang, C. P. Huang, C. Ma, X. L. Song, Q. J. Xu, *J. Mater. Chem.*, 2012, 22, 4050-4055.

[15] L. Ge, C. C. Han, J. Liu, *Appl. Catal. B: Environ.* 2011, 108-109, 100-107.

[16] M. Hojamberdieva, R. M. Prasada, K. Moritaa, Y. F. Zhu, M. A. Schiavond, A. Gurloa, R. Riedel, *Appl. Catal. B: Environ.* 2012, 115-116, 303-313.

[17] C. Lettmann, H. Hinrichs, W. F. Maier, *Angew. Chem.*, 2001, 113, 3258-3262; *Angew. Chem. Int. Ed.*, 2001, 40, 3160-3164.

[18] N. Serpone, *J. Phys. Chem. B*, 2006, 110, 24287-24293.

[19] Y. T. Liang, B. J. K. Vijayan, O. Lyandres, K. A. Gray, M. C. Hersam, *J. Phys. Chem. Lett.*, 2012, 3, 1760-1765.

[20] Z. G. Yi, J. H. Ye, N. Kikugawa, T. Kako, S. X. Ouyang, H. S. Williams, H.

Yang, J. Y. Cao, W. J. Luo, Z. S. Li, Y. Liu, R. L. Withers, *Nat. Mater.*, 2010, 9, 559-564.

[21] H. F. Shi, X. L. Huang, H. M. Tian, J. Lv, Z. S. Li, J. H. Ye, Z. G. Zou, *J. Phys. D: Appl. Phys.*, 2009, 42, 1-6.

[22] H. F. Shi, Z. S. Li, J. H. Ye, Z. G. Zou, *J. Phys. D: Appl. Phys*. 2010, 43, 085402.

[23] T. Nakato, H. Ueda, S. Hashimoto, R. Terao, M. Kameyama, E. Mouri, *ACS Appl. Mater. Interfaces*, 2012, 4, 4338-4347.

[24] H. F. Shi, G. Q. Chen, Z. G. Zou, *Appl. Catal. B. Environ.*, 2014, 156-157, 378-384.

[25] R. Konta, H. Kato, H. Kobayashi, A. Kudo, *Phys. Chem. Chem. Phys.*, 2003, 5, 3061-3065.

[26] X. X. Hu, C. Hu, *J. Solid State Chem.*, 2007, 180, 725-732.

[27] H. Xu, H. M. Li, L. Xu, C. D. Wu, G. S. Sun, Y. G. Xu, J. Y. Chu, *Ind. Eng. Chem. Res.*, 2009, 48, 10771-10778.

[28] A. Singh, D. P. Dutta, A. Ballal, A. K. Tyagi, M. H. Fulekar, *Mater. Res. Bull.*, 2014, 51, 447-454.

[29] Q. Zhu, W. S. Wang, L. Lin, G. Q. Gao, H. L. Guo, H. Du, A.W. Xu, *J. Phys. Chem. C*, 2013, 117, 5894-5900.

[30] S. B. Yang, Y. J. Gong, J. S. Zhang, L. Zhan , L. L. Ma , Z. Y. Fang, R. Vajtai , X. C. Wang , P. M. Ajayan, *Adv. Mater.*, 2013, 25, 2452-2456.

[31] X. Wang, K. Maeda, X. Chen, K. Takanabe, K. Domen, Y. Hou, X. Fu, M. J. Antonietti, *J. Am. Chem. Soc.*, 2009, 131, 168-1681.

[32] Z. Ding, X. Chen, M. Antonietti, X. Wang, *ChemSusChem*, 2011, 4, 274-281.

[33] Y. Di, X. Wang, A. Thomas, M. Antonietti, *ChemCatChem*, 2010, 2, 834-838.

[34] G. H. Dong, L. Z. Zhang, *J. Mater. Chem.*, 2012, 22, 1160-1166.

[35] X. Wang, A. Maeda, K. Thomas, G. Takanabe, J.M. Xin, K. Carlsson, Domen, M. Antonietti,. *Nat. Mater.*, 2009, 8, 76-82.

[36] S. Kumar, T. Surendar, A. Baruah, V. Shanker, *J. Mater. Chem. A*, 2013, 1, 5333-5340.

[37] J. Y. Zhang, Y. H. Wang, J. Jin, J. Zhang, Z. Lin, F. Huang, J. G. Yu, *ACS Appl. Mater. Interfaces*, 2013, 5, 10317-10324.

[38] C. S. Pan, J. Xu, Y.J. Wang, D. Li, Y. F. Zhu, *Adv. Funct. Mater.*, 2012, 22, 1518-1524.

[39] H. F. Shi, G. Q. Chen, C. L. Zhang, Z. G. Zou, *ACS Catal.*, 2014, 4,

3637–3643.

[40] L. M. Sun, X. Zhao, C. J. Jia, Y. X. Zhou, X. F. Cheng, P. Li, L. Liu, W. L. Fan, *J. Mater. Chem.*, 2012, 22, 23428-23438.

[41] Y. P. Yuan, S. W. Cao, Y. S. Liao, L. S. Yin, C. Xue, *Appl. Catal. B: Environ*, 2013, 140-141, 164-168.

[42] F. Chang, Y. Xie, J. Zhang, J. Chen, C. Li, J. Wang, J. Luo, B. Deng, X. Hu, *RSC Adv*., 2014, 4, 28519–28528.

[43] W. Zhao, Y. Guo, S. Wang, H. He, C. Sun, S. G. Yang, *Appl. Catal. B. Environ.,* 2015*,* 165, 335–343.

[44] H. F. Shi, T. Z. Wang, J. Chen, C. Zhu, J. H. Ye, Z. G. Zou, *Catal. Lett.*, 2011, 141, 525-530.

[45] D. F. Wang, A. Pierre, M. G. Kibria, K. Cui, X. G. Han, K. H. Bevan, H. Paradis, S. Guo, A. R. Hakima, Z. T. Mi, *Nano Lett.*, 2011, 11, 2353-2357.

[46] H. L. Zhou, Y. Q. Qu, T. Zeid, X. F. Duan, *Energy. Environ. Sci*., 2012, 5, 6732-6743.

[47] Y. Wang, X. Wang, Antonietti, M. Antonietti, *Angew*. *Chem. Int. Ed.*, 2012, 51, 68-89.

[48] A. Vinu, *Adv. Funct. Mater.*, 2008, 18, 816-827.

[49] Q. J. Xiang, J. G. Yu, M. J. Jaroniec, *J. Phys. Chem. C.*, 2011, 115, 7355-7363.

[50] J. X. Sun, Y. P. Yuan, L. G. Qiu, X. Jiang, A. J. Xie, Y. H. Shen, J. F. Zhu, *Dalton Trans.*, 2012, 41, 6756-6763.

[51] S. M. Wang, D. L. Li, C. Sun, S. G. Yang, Y. Guan, H. He, *Appl. Catal. B. Environ.,* 2014, 4, 885– 892

[52] W. Liu, X. Liu, Y. Fu, Q. You, R. Huang, P. Liu, Z. Li, *Appl. Catal. B Environ.* 2012, 123, 78–83.

[53] C. Zhang, Y. Zhu, *Chem. Mater.*, 2005, 17, 3537-3545.

[54] C. Huang, L. Chen, K. W. Cheng, G.T. Pan, *J. Mol. Catal. A*, 2007, 261, 218-224.

[55] A. H. Nethercot, *Phys. Rev. Lett.*, 1974, 33, 1088.

[56] M. A. Butler, D. S. Ginley, *J. Electrochem. Soc.*, 1978, 125, 228.

[57] H. F Shi, Z. S. Li, J. H. Kou, J. H. Ye, Z. G, Zou, *J. Phys. Chem. C*, 2011, 115, 145-151.

[58] C.H Chen, Q.W Liu, S.M. Gao, K.i Li, H. Xu, Z. Z. Lou, B.B. Huang, Y. Dai, *RSC Adv*, 2014, 4, 12098-12104

[59] P. Wang, B. Huang, X. Qin, X. Zhang, Y. Dai, J. Wei, M. H. Whangbo, *Angew.*

Chem., Int. Ed., 2008, 47, 7931.

[60] C. Hu, T. Peng, X. Hu, Y. Nie, X. Zhou, J. Qu, H. He, *J. Am. Chem. Soc.,* 2010, 132, 857.

[61] P. Wang, B. Huang, X. Zhang, X. Qin, Y. Dai, Z. Wang, J. Wei, J. Zhan, S. Wang, J. Wang and M. H. Whangbo, *Chem. Eur. J.*, 2009, 15, 1821.

[62] Q. Zhu, W.S. Wang, L. Lin, G. Q. Gao, H. L. Guo, H. Du, A.W. Xu, *J. Phys. Chem. C* 2013, 117, 5894–5900.

[63] C. An, S. Peng, Y. Sun, *Adv. Mater*., 2010, 22, 2570.

[64] Y. Bu, Z.Y. Chen, C. Feng, W.B. Li, *RSC Adv.,* 2014, 4, 38124–38132

[65] S.W. Zhang, J.X. Li,, X.K. Wang, Y.S. Huang, M.Y. Zeng, J.Z. Xu, *ACS Appl. Mater. Interfaces* 2014, 6, 22116-22125

[66] Y. J. Wang, R. Shi, J. Lin, Y. F. Zhu, *Energy Environ. Sci.*, 2011, 4, 2922-2929.

[67] C. S. Pan, J. Xu, Y. J. Wang, D. Li, Y. F. Zhu, *Adv. Funct. Mater.*, 2012, 22, 1518-1524.

[68] Shi, H. F.; Li, X. K.; Wang, D. F.; Yuan, Y. P.; Zou, Z. G.; Ye, J. H. *Catal. Lett.* 2009, 132, 205−212.

Figure captions

Fig. 1. XRD patterns of g-C_3N_4, $AgVO_3$, and g-C_3N_4/$AgVO_3$ composite photocatalysts.

Fig. 2. (a) UV-vis diffuse reflectance spectra of g-C_3N_4, $AgVO_3$, and g-C_3N_4/$AgVO_3$ composite photocatalysts and (b) plots of $(\alpha hv)^{1/2}$ versus energy (b) of $AgVO_3$ and g-C_3N_4.

Fig. 3. XPS spectra of the samples: (a) C 1s peaks of g-C_3N_4/0.2$AgVO_3$ and g-C_3N_4; (b) N 1s peaks of g-C_3N_4/0.2$AgVO_3$ and g-C_3N_4; (c) Ag 3d peaks of $AgVO_3$ and g-C_3N_4/0.2$AgVO_3$; (d) O 1s peaks of $AgVO_3$ and g-C_3N_4/0.2$AgVO_3$; (e) V 2p peaks of $AgVO_3$ and g-C_3N_4/0.2$AgVO_3$.

Fig. 4. FE-SEM images of (a) g-C_3N_4, (b) $AgVO_3$, and (c) g-C_3N_4/0.2$AgVO_3$.

Fig. 5. (a) Low- and (b) high-magnification transmission electron microscopy (TEM) images of g-C_3N_4/0.2$AgVO_3$ composite.

Fig. 6. Photocatalytic activities of g-C_3N_4, $AgVO_3$, physically mixed C_3N_4-$AgVO_3$, and g-C_3N_4/0.2$AgVO_3$ composite photocatalysts for degrading RhB under visible light irradiation.

Fig. 7. Reaction cycling runs for the photocatalytic degradation of RhB over g-C_3N_4/0.2$AgVO_3$ composite under visible light irradiation.

Fig. 8. XRD patterns for g-C_3N_4/0.2$AgVO_3$ composite photocatalyst before and after photocatalytic reaction.

Fig. 9. First-order kinetics for the photodegradation of RhB over g-C_3N_4, $AgVO_3$, physically mixed C_3N_4-$AgVO_3$, and g-C_3N_4/$AgVO_3$ samples under visible light irradiation. The inset is the rate constant k of the photodegradation of RhB over g-C_3N_4, $AgVO_3$, physically mixed C_3N_4-$AgVO_3$, and g-C_3N_4/$AgVO_3$ samples.

Fig. 10. Valence band (VB) XPS spectra of g-C_3N_4 and $AgVO_3$.

Fig. 11. Schematic diagram of the separation and transfer of photogenerated charges in the Ag/C_3N_4/$AgVO_3$ composite under visible light irradiation.

Fig. 12. Photoluminescence (PL) spectra of g-C_3N_4 and g-C_3N_4/0.2$AgVO_3$.

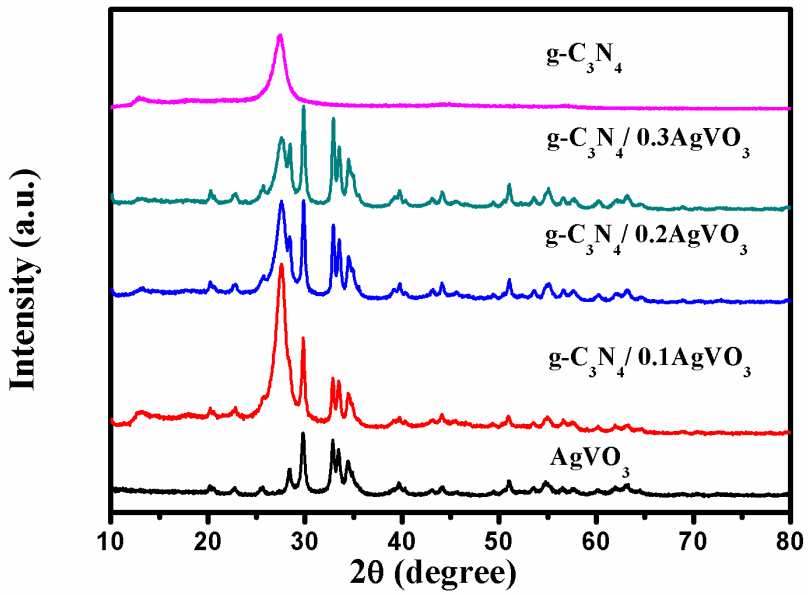
g-C3N4
g-C3N4 / 0.3AgVO3
g-C3N4 / 0.2AgVO3
g-C3N4 / 0.1AgVO3
AgVO3
Intensity (a.u.)
10
20
30
40
50
60
70
80
2θ (degree)

Fig. 1.

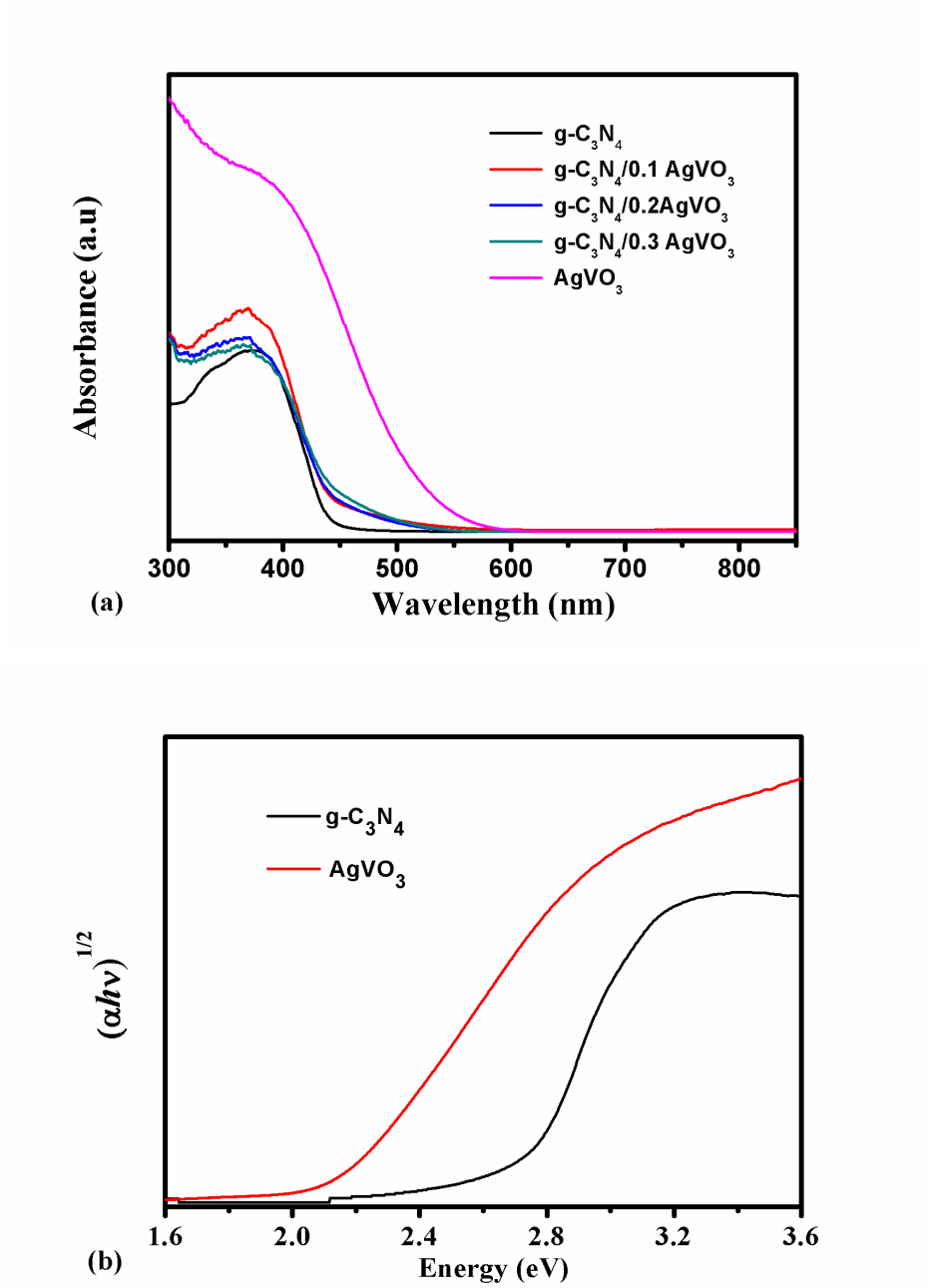
g-C3N4
g-C3N4/0.1 AgVO3
g-C3N4/0.2AgVO3
g-C3N4/0.3 AgVO3
AgVO3
Absorbance (a.u)
300
400
500
600
700
800
Wavelength (nm)
(a)
g-C3N4
AgVO3
(αhν)1/2
1.6
2.0
2.4
2.8
3.2
3.6
Energy (eV)
(b)

Fig. 2.

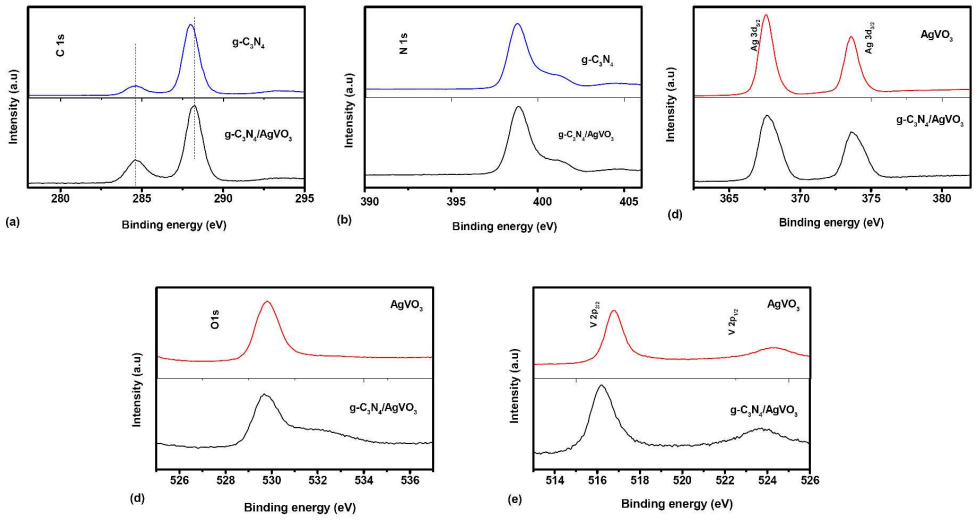
C 1s
g-C3N4
g-C3N4/AgVO3
Intensity (a.u)
280
285
290
295
Binding energy (eV)
(a)
N 1s
g-C3N4
g-C3N4/AgVO3
Intensity (a.u)
390
395
400
405
Binding energy (eV)
(b)
Ag 3d3/2
Ag 3d5/2
AgVO3
g-C3N4/AgVO3
Intensity (a.u)
365
370
375
380
Binding energy (eV)
(d)
O1s
AgVO3
g-C3N4/AgVO3
Intensity (a.u)
526
528
530
532
534
536
Binding energy (eV)
(d)
V 2p1/2
V 2p3/2
AgVO3
g-C3N4/AgVO3
Intensity (a.u)
514
516
518
520
522
524
526
Binding energy (eV)
(e)

Fig. 3.

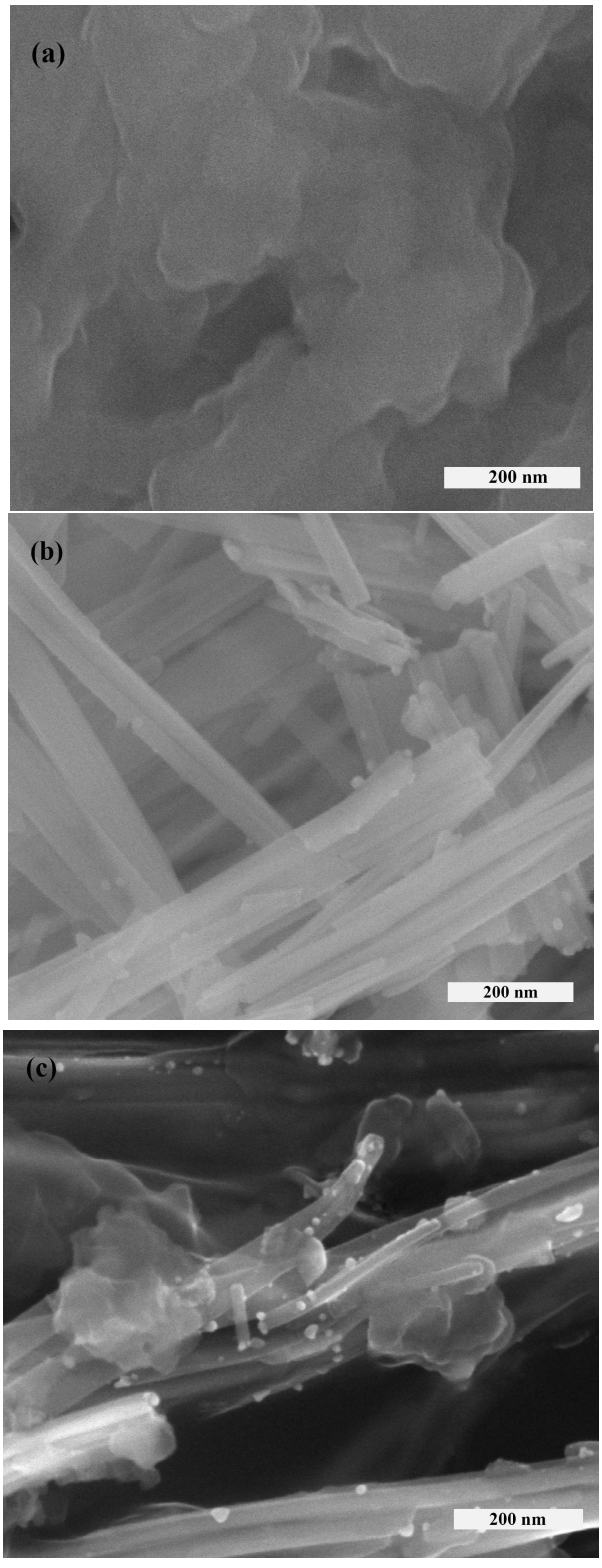

Fig. 4.

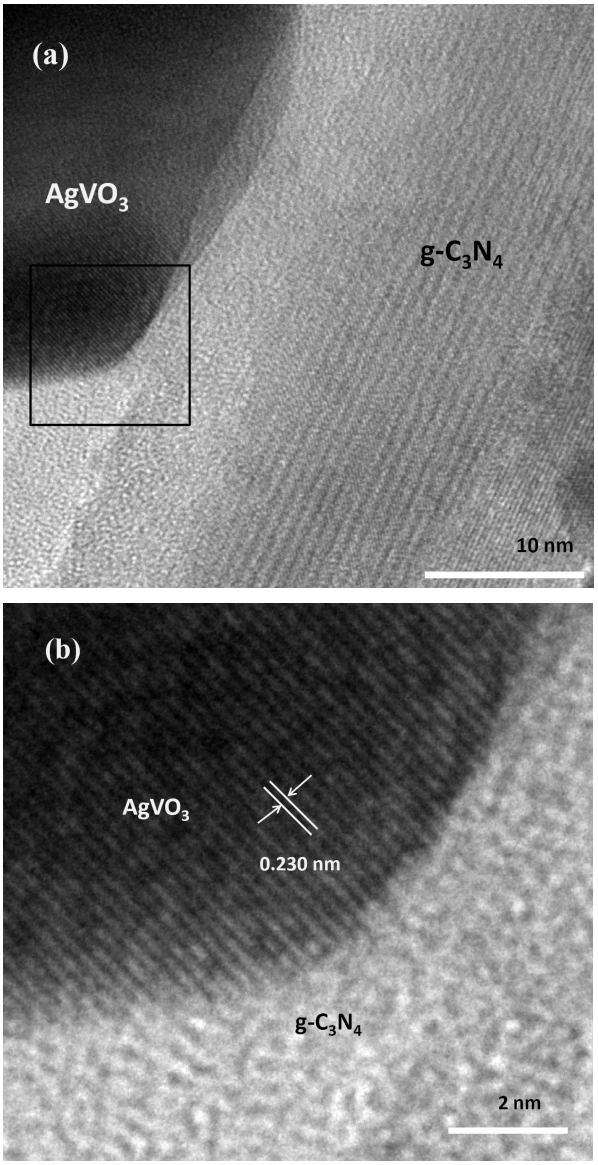

Fig. 5.

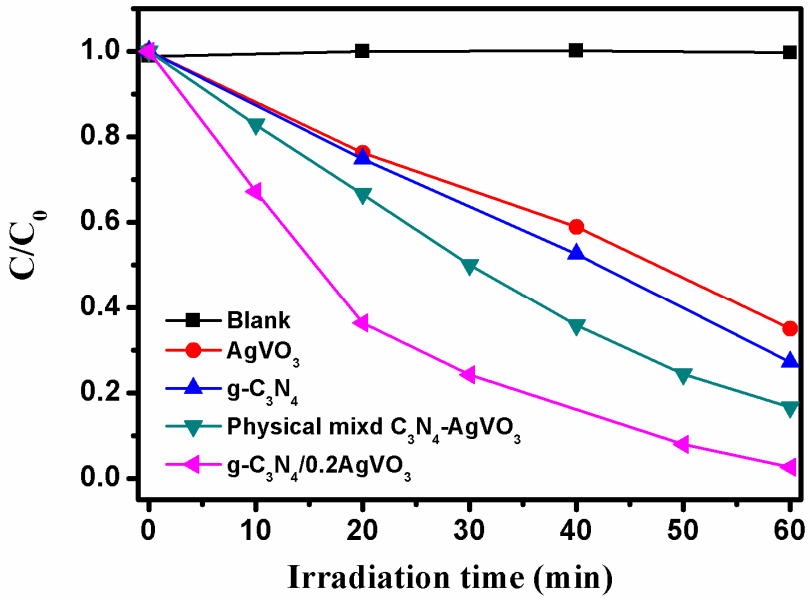
C/C0
1.0
0.8
0.6
0.4
0.2
0.0
0
10
20
30
40
50
60
Irradiation time (min)
Blank
AgVO3
g-C3N4
Physical mixd C3N4-AgVO3
g-C3N4/0.2AgVO3

Fig. 6.

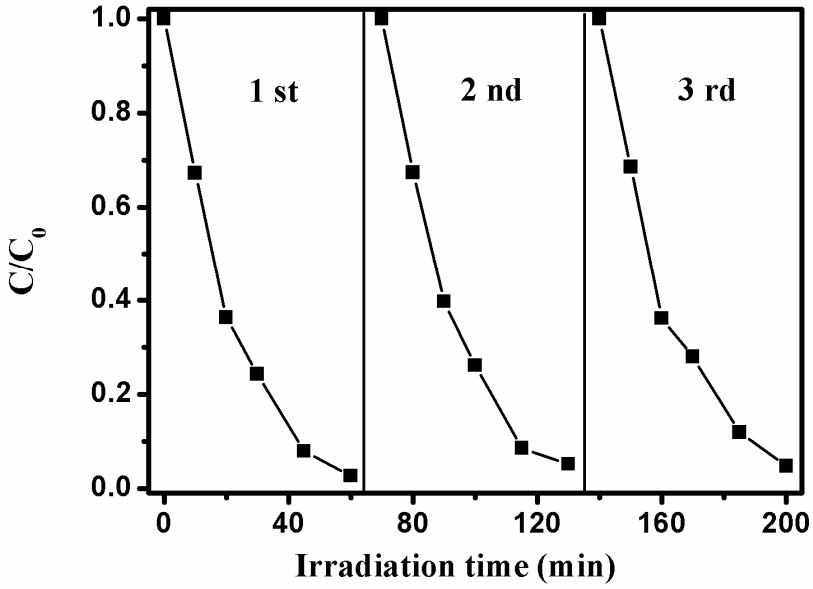
1.0
0.8
0.6
0.4
0.2
0.0
C/C0
1 st
2 nd
3 rd
0
40
80
120
160
200
Irradiation time (min)

Fig. 7.

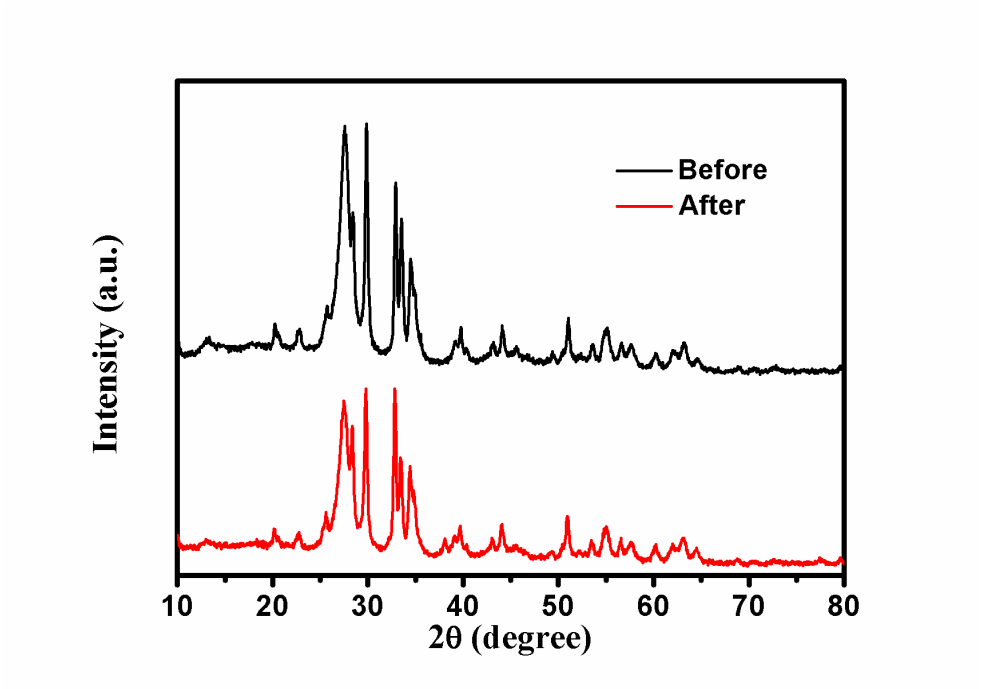

Fig. 8.

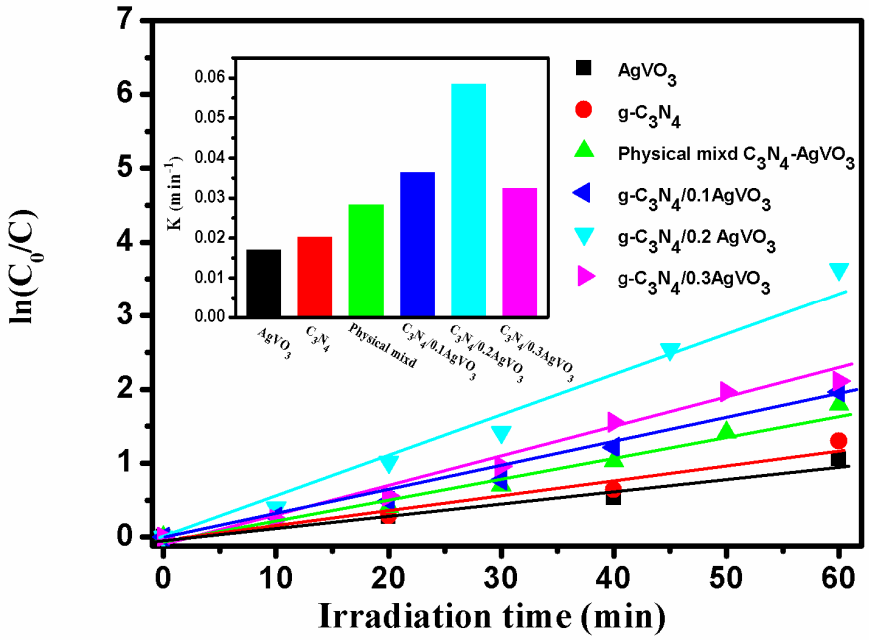
ln(C0/C)
Irradiation time (min)
AgVO3
g-C3N4
Physical mixd C3N4-AgVO3
g-C3N4/0.1AgVO3
g-C3N4/0.2 AgVO3
g-C3N4/0.3AgVO3
K (min-1)
AgVO3
C3N4
Physical mixd
C3N4/0.1AgVO3
C3N4/0.2AgVO3
C3N4/0.3AgVO3

Fig. 9.

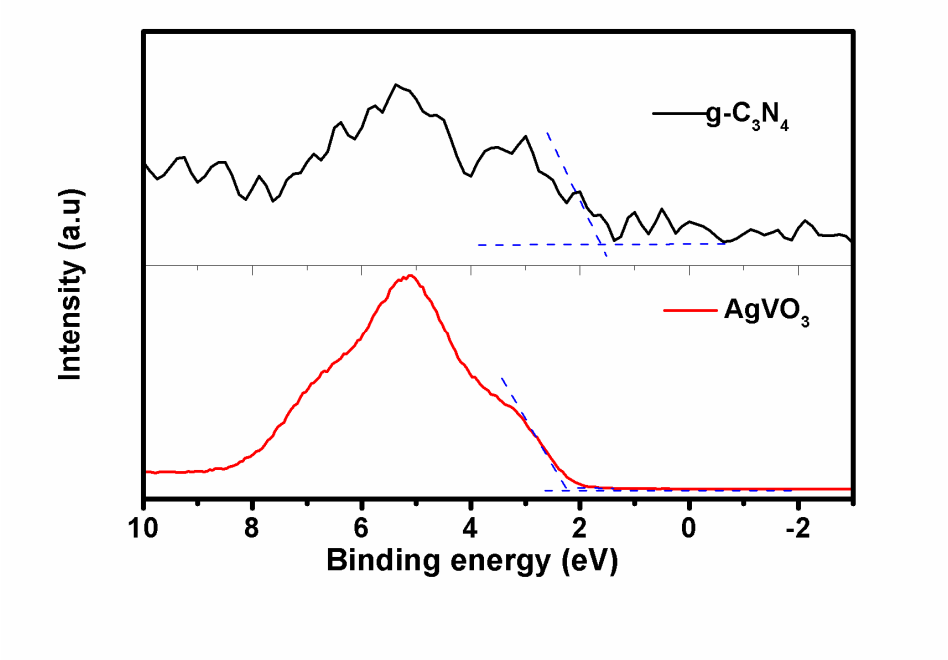

Fig. 10.

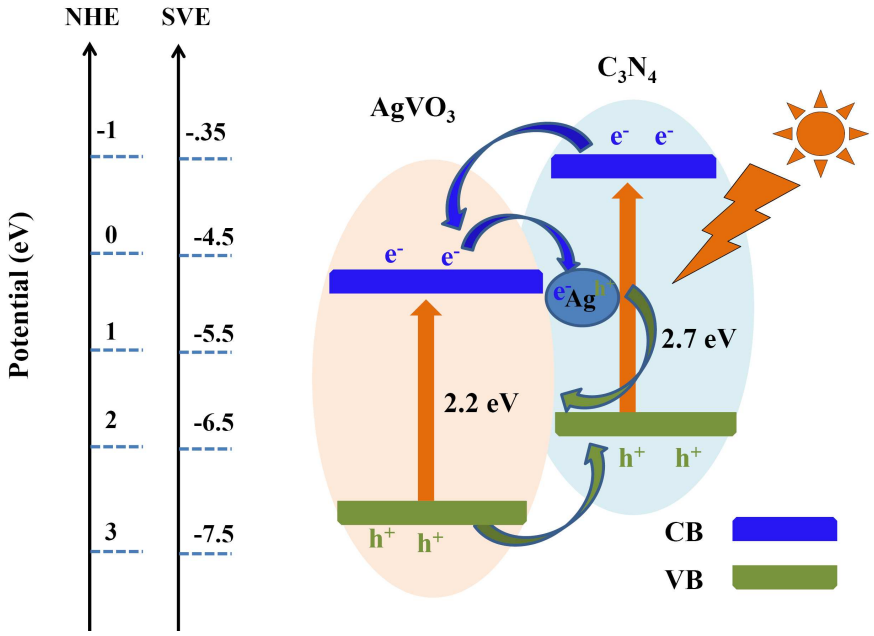
NHE
SVE
Potential (eV)
-1
-.35
0
-4.5
1
-5.5
2
-6.5
3
-7.5
AgVO3
C3N4
e- e-
e- e-
e- Ag
2.7 eV
2.2 eV
h+ h+
h+ h+
CB
VB

Fig. 11.

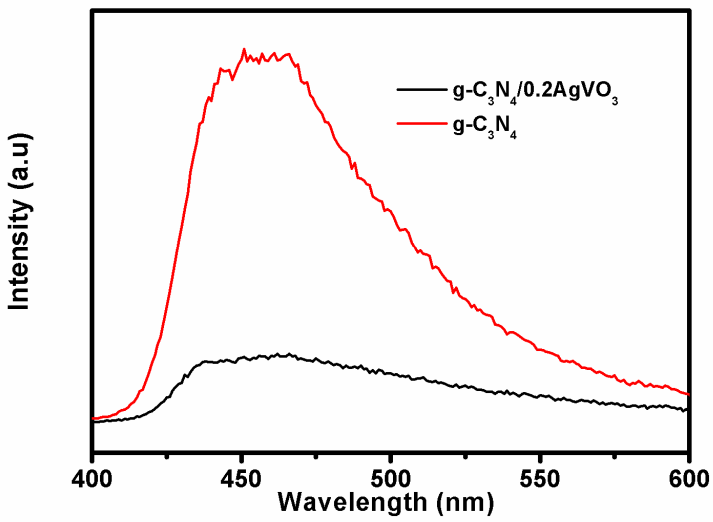
g-C3N4/0.2AgVO3
g-C3N4
Intensity (a.u)
400
450
500
550
600
Wavelength (nm)

Fig. 12

Graphical Abstract